

## NUMERICAL MODELING OF THE SOLIDIFICATION PROCESS IN A MOLD-CASTING SYSTEM WITH A GASEOUS GAP

*Ewa Węgrzyn-Skrzypczak<sup>1</sup>, Tomasz Skrzypczak<sup>2</sup>, Leszek Sowa<sup>2</sup>*

*<sup>1</sup> Department of Mathematics, Czestochowa University of Technology  
Czestochowa, Poland*

*<sup>2</sup> Department of Mechanics and Fundamentals of Machine Design, Czestochowa University  
of Technology, Czestochowa, Poland*

*ewa.wegrzyn-skrzypczak@pcz.pl, tomasz.skrzypczak@pcz.pl, leszek.sowa@pcz.pl*

Received: 9 December 2024; Accepted: 6 March 2025

**Abstract.** The paper focuses on the numerical modeling of the solidification process, with particular emphasis on the key physical phenomenon of heat transfer within the mold-casting system. This process is influenced by the presence of a gaseous gap, which introduces thermal resistance at the interface and affects the solidification rate. The numerical model is developed using the Finite Element Method (FEM), with separate spatial discretizations for both the casting and the mold. Additionally, the thermal expansion of these regions, caused by temperature-dependent volume changes, is accounted for. The model utilizes two distinct meshes to compute the evolving temperature fields. Heat exchange between the casting and the mold is governed by boundary conditions linking the two regions. The solution is computed incrementally, with each region being solved independently at each time step. This paper describes the main assumptions of the mathematical and numerical models and presents the comparison of results of three simulation variants carried out using a custom-built program.

*MSC 2010: 65M60, 68U20*

*Keywords: numerical modeling, finite element method, solidification process, heat transfer, gaseous gap*

### 1. Introduction

Numerical modeling using the finite element method (FEM) and computer simulations is widely used in many industrial branches. Analysis of temperature, strain and stress distribution in manufactured components and tools is an important part of modeling various processes and physical phenomena, such as wire drawing [1] or solidification. The course and characteristics of the solidification process often determine the quality and performance of cast parts. One of the important phenomena influencing this process is the formation of a gas gap at the interface between the

casting and the mold, often called an "air gap". Thermal shrinkage and other thermo-mechanical effects during the cooling process are the main causes of its presence. This phenomenon significantly affects the heat transfer between the casting and the mold and obviously the cooling rate of the casting.

The influence of the air gap on the solidification process and heat transfer is widely discussed in the literature. Paper [2] investigated the air gap formation process for cylindrical and flat castings. It focused on the effect of the time-variable gap width during solidification and its influence on the heat transfer through the mold-casting interface. A thermomechanical model to analyze the air gap formation during continuous casting, paying attention to the effect of mold geometry modification on the thermal resistance of the gap was presented in [3]. Mortensen et al. [4] did a study on the coupled modeling of air gap formation and surface exudation during the casting of aluminum extrusion ingots. Their findings showed that the pull-in force at the surface significantly enlarges the air gap near the mold during the initial stages of solidification. Additionally, they examined the influence of surface exudation on both the heat transfer process and the resulting microstructural development. Zeng et al. [5] investigated the effect of the air gap width and its formation time on the heat transfer coefficient (HTC) at the mold-casting interface, showing that the HTC decreases significantly with the increase of the gap width. Ahmadein et al. [6] further investigated the relationship between HTC and local gap size, showing that heat transfer is highly dependent on the contact pressure and thermal conditions at the interface. Xu et al. [7] simulated the directional solidification process using a multilayer mold that was gradually immersed in water after the filling step. Their results indicated that this approach improves heat transfer by minimizing the formation of an air gap, leading to better grain structures and improved mechanical properties of the castings. Similarly, Li et al. [8] investigated the formation of an air gap during the casting of steel ingots and its effect on interfacial heat transfer. They observed that the air gap develops earlier and becomes more visible on the narrower side of the ingot compared to the wider side. Furthermore, they introduced a simple equation to estimate the HTC by taking into account conduction, radiation, and thermal resistance at the gap. The research presented in [9] analyzed the heat transfer during the solidification process considering the influence of different mold materials. It has been shown that the properties of the mold material significantly affect the HTC, cooling rate and total solidification time.

In this study, the solidification process in the mold-casting system is analyzed numerically, with special attention paid to the role of the air gap. To capture the effect of the phenomenon on the solidification process, three series of numerical calculations were carried out: solidification with an air gap, the width of which is recalculated at each time step based on the thermal deformations of the casting and mold, solidification with an air gap of constant width and solidification with an almost ideal contact (the gap width tends to 0). The effect of the air gap width on heat transfer was investigated by comparing obtained results, which is important

from the point of view of improving the cooling conditions in the casting processes and increasing the quality of cast products.

## 2. Mathematical and numerical descriptions

Figure 1 illustrates the schematic representation of the general case of the problem, where the domain is divided into two regions:  $\Omega_M$ , representing the mold, and  $\Omega_C$ , representing the solidifying alloy. During the liquid-to-solid phase transition, thermal contraction of both casting and mold occurs, resulting in the formation of a gap between the boundaries  $\Gamma_M$  and  $\Gamma_C$ . The gap width, denoted as  $h$ , varies with time, and its thermal resistance significantly impacts heat transfer between the casting and the mold. Heat is also transported to the environment through external surfaces of the mold and the top surface of the casting. To simplify the calculations, only a quarter of the mold-casting system is considered, taking advantage of symmetry. Thermal insulation is applied along the  $xy$  and  $yz$  symmetry planes. Additionally, the displacement boundary conditions are defined as follows:  $z = 0$  on the  $xy$  plane,  $x = 0$  on the  $yz$  plane, and  $x = y = z = 0$  at the fixed point  $A$ .

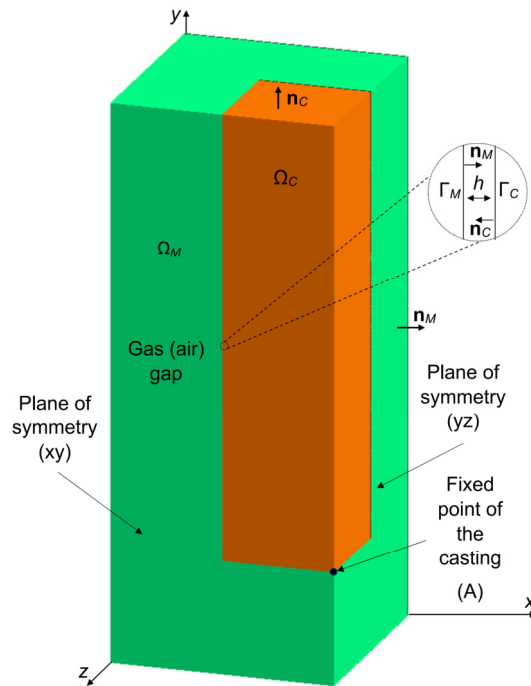


Fig. 1. Scheme of a quarter of mold-casting system

The mathematical model of the problem includes an equation describing heat transport in the casting and the mold, as well as a set of equations describing displacements in these regions:

$$\frac{\partial}{\partial x} \left( \lambda^{(i)} \frac{\partial T^{(i)}}{\partial x} \right) + \frac{\partial}{\partial y} \left( \lambda^{(i)} \frac{\partial T^{(i)}}{\partial y} \right) + \frac{\partial}{\partial z} \left( \lambda^{(i)} \frac{\partial T^{(i)}}{\partial z} \right) = c^{(i)} \rho^{(i)} \frac{\partial T^{(i)}}{\partial t} \quad (1)$$

$$\begin{aligned} f_1 \frac{\partial^2 u_x^{(i)}}{\partial x^2} + f_2 \left( \frac{\partial^2 u_y^{(i)}}{\partial x \partial y} + \frac{\partial^2 u_z^{(i)}}{\partial x \partial z} \right) + f_3 \left( \frac{\partial^2 u_x^{(i)}}{\partial y^2} + \frac{\partial^2 u_x^{(i)}}{\partial z^2} + \frac{\partial^2 u_y^{(i)}}{\partial y \partial x} + \frac{\partial^2 u_z^{(i)}}{\partial z \partial x} \right) + f_4 a^{(i)} \Delta T^{(i)} &= 0 \\ f_1 \frac{\partial^2 u_y^{(i)}}{\partial y^2} + f_2 \left( \frac{\partial^2 u_x^{(i)}}{\partial y \partial x} + \frac{\partial^2 u_z^{(i)}}{\partial y \partial z} \right) + f_3 \left( \frac{\partial^2 u_x^{(i)}}{\partial x \partial y} + \frac{\partial^2 u_y^{(i)}}{\partial x^2} + \frac{\partial^2 u_y^{(i)}}{\partial z^2} + \frac{\partial^2 u_z^{(i)}}{\partial z \partial y} \right) + f_4 a^{(i)} \Delta T^{(i)} &= 0 \\ f_1 \frac{\partial^2 u_z^{(i)}}{\partial z^2} + f_2 \left( \frac{\partial^2 u_x^{(i)}}{\partial z \partial x} + \frac{\partial^2 u_y^{(i)}}{\partial z \partial y} \right) + f_3 \left( \frac{\partial^2 u_x^{(i)}}{\partial x \partial z} + \frac{\partial^2 u_y^{(i)}}{\partial y \partial z} + \frac{\partial^2 u_z^{(i)}}{\partial x^2} + \frac{\partial^2 u_z^{(i)}}{\partial y^2} \right) + f_4 a^{(i)} \Delta T^{(i)} &= 0 \end{aligned} \quad (2)$$

The coefficients  $f_1, f_2, f_3$ , and  $f_4$  are shown below:

$$\begin{aligned} f_1 &= \frac{E^{(i)}(1-\nu^{(i)})}{(1+\nu^{(i)})(1-2\nu^{(i)})}, & f_2 &= \frac{E^{(i)}\nu^{(i)}}{(1+\nu^{(i)})(1-2\nu^{(i)})} \\ f_3 &= \frac{E^{(i)}}{2(1+\nu^{(i)})}, & f_4 &= \frac{E^{(i)}(1+\nu^{(i)})}{(1+\nu^{(i)})(1-2\nu^{(i)})} \end{aligned} \quad (3)$$

The variables employed in the proposed model include: thermal conductivity coefficient  $\lambda$  [ $\text{J s}^{-1} \text{m}^{-1} \text{K}^{-1}$ ], heat capacity  $c$  [ $\text{J K}^{-1} \text{kg}^{-1}$ ], density  $\rho$  [ $\text{kg m}^{-3}$ ], temperature  $T$  [K], time  $t$  [s], Cartesian coordinates  $x, y, z$  [m], and the index  $i$ , which specifies the  $i$ -th region. It is important to emphasize that the index  $i$  identifies either the casting ( $C$ ) or the mold ( $M$ ). Furthermore, the components of the displacement vector are represented as  $u_x, u_y$ , and  $u_z$  [m]. Additional parameters appearing in the equations include Young's modulus  $E$  [ $\text{N m}^{-2}$ ], Poisson's ratio  $\nu$  [-], the linear thermal expansion coefficient  $a$  [ $\text{K}^{-1}$ ], and the temperature difference  $\Delta T$  [K], calculated as  $\Delta T = T - T_{ref}$ , where  $T_{ref}$  [K] denotes the reference temperature. The formula describing heat capacity  $c$  below the solidus temperature  $T_S$ , above the liquidus temperature  $T_L$ , and between  $T_S$  and  $T_L$ , as well as the boundary and initial conditions and the mathematical operations leading to equation (2), are derived in detail in [10].

The numerical model is formulated using the Finite Element Method (FEM) and the Galerkin method. Equations (1) and (2) are spatially discretized, while equation (1) is also temporally discretized using the backward Euler scheme. A detailed numerical approach is provided in [10]. The final form of the global FEM equations is presented below:

$$\mathbf{K}_T^{(i)} \mathbf{T}_{f+1}^{(i)} + \mathbf{M}_T^{(i)} \frac{\mathbf{T}_{f+1}^{(i)} - \mathbf{T}_f^{(i)}}{\Delta t} = \mathbf{B}_T^{(i)} \quad (4)$$

$$\mathbf{K}_D^{(i)} \mathbf{u}^{(i)} = \mathbf{B}_D^{(i)} \quad (5)$$

where  $\mathbf{K}_T$  represents the thermal conductivity matrix, while  $\mathbf{M}_T$  denotes the thermal capacity matrix. The vector  $\mathbf{B}_T$  stores the thermal boundary conditions, and  $\mathbf{T}$  contains the unknown nodal temperatures at the time steps  $f$  and  $f+1$ . In Equation (5),  $\mathbf{K}_D$  denotes the stiffness matrix,  $\mathbf{B}_D$  is the vector containing known boundary displacements, and  $\mathbf{u}$  is the vector containing the unknown nodal displacements. At each iteration step, the solution for equation (4) is independently obtained for both the casting and the mold. The resulting temperatures are then used to calculate the thermal deformations in both regions using equation (5).

### 3. Examples of calculation

The geometry of the mold-casting system is prepared in the GMSH software. The mold is a rectangular prism with dimensions of  $0.2 \times 0.2 \times 0.25$  m, while the casting takes the form of a prism with dimensions  $0.1 \times 0.1 \times 0.2$  m. Only one-quarter of the system is considered (Fig. 1). The mold is initially at a temperature of 400 K and filled with molten bronze at 1350 K. Convective heat transfer conditions are applied to the external surfaces of the mold and the top surface of the casting, with a heat transfer coefficient of  $\alpha = 100 \text{ J s}^{-1} \text{ m}^{-2} \text{ K}^{-1}$  and an ambient temperature of 300 K. A constant time step of  $\Delta t = 0.1$  s is used. The material properties of the mold-casting system are provided in Table 1. Physical properties are generally temperature dependent, but determining this dependence is difficult. For this reason, certain simplifications are sometimes used in numerical modeling of heat flow [11].

Table 1. Material properties used in the simulations

Material property	Casting		Mold	Air gap
	Liquid phase	Solid phase		
$\lambda$ [ $\text{J s}^{-1} \text{ m}^{-1} \text{ K}^{-1}$ ]	25	46	45	0.2
$c$ [ $\text{J K}^{-1} \text{ kg}^{-1}$ ]	540	440	753	–
$\rho$ [ $\text{kg m}^{-3}$ ]	8300	8900	7200	–
$E$ [ $\text{N m}^{-2}$ ]	–	$8.3 \cdot 10^{10}$	$9.0 \cdot 10^{10}$	–
$\nu$ [–]	–	0.34	0.21	–
$\alpha$ [ $\text{K}^{-1}$ ]	–	$1.8 \cdot 10^{-5}$	$1.04 \cdot 10^{-5}$	–
$T_L$ [K]	1298		–	–
$T_S$ [K]	1243		–	–
$L$ [ $\text{J kg}^{-1}$ ] (latent heat)	$2.2 \cdot 10^5$		–	–

Three computer simulations are performed using custom-developed software, followed by the comparison of the temperature distributions within the mold-casting system and the fraction of the solid phase in the casting. Thermally deformed regions are also presented in the first simulation case. Each simulation employed a different approach to modeling the gas gap between the casting and the mold. In the first simulation, the gap was modeled dynamically, taking into account the thermal deformations of both the mold and the casting over time, resulting in a gap width that varied spatially and temporally. The second simulation assumed a fixed gap width, averaged from the dynamic gap width observed at the midpoint of the solidification process in the first simulation ( $h = 1.5 \cdot 10^{-4}$  m). The third simulation represented a near-perfect contact scenario, with the gap width set to  $h = 10^{-9}$  m.

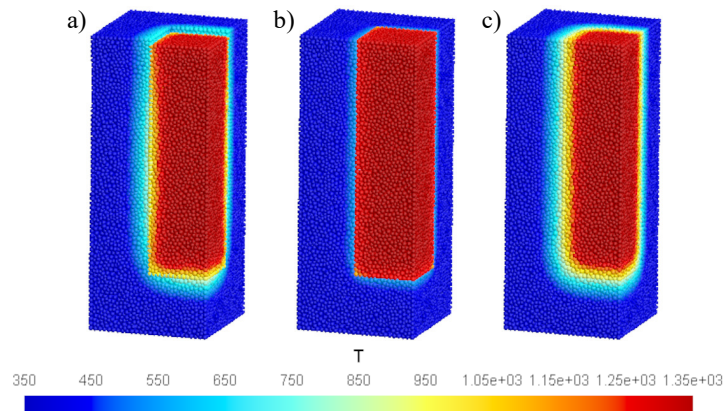


Fig. 2. Temperature distribution at 10 s in the three simulation scenarios

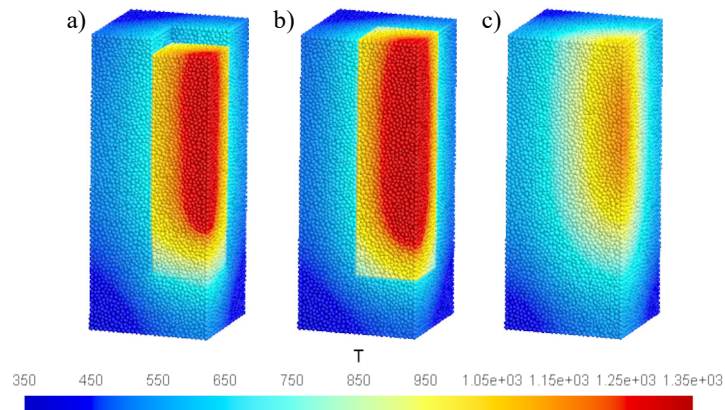


Fig. 3. Temperature distribution at 115 s in the three simulation scenarios

Comparing the temperature distributions at two selected moments, it is evident that the thermal resistance at the interface between the casting and the mold is highest at the beginning of the solidification process in the case with a constant gas

gap width (Fig. 2b). In contrast, in the scenario with nearly perfect contact, a continuous temperature distribution across the contact interfaces is observed, indicating the most efficient heat transfer (Fig. 2c). After 115 s, it is noticeable that in the third case (Fig. 3c), the casting is the most cooled, while in the second case, it is the least (Fig. 3b). The case with a dynamically calculated gap falls in the middle, even though at this stage, the gas gap is significantly wider than it is in the second case, resulting in greater thermal resistance (Fig. 3a).

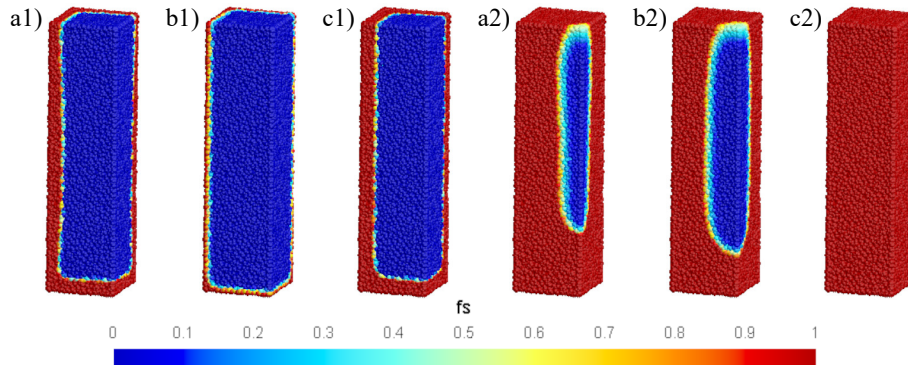


Fig. 4. Solid fraction distribution at 10 s (a1-c1) and 115 s (a2-c2) for the three simulation scenarios

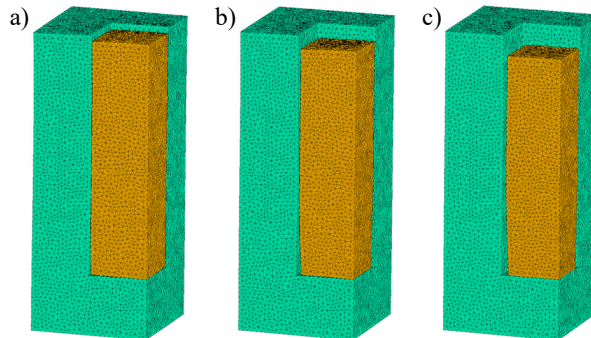


Fig. 5. Thermal deformations (magnified 10x) of the casting and the mold in the first simulation scenario at 10 s (a), 80 s (b), and 165 s (c)

The conclusions derived from the temperature field analysis confirm the solid fraction distributions presented in Figure 4. It is clearly visible that, after 115 s, the third case shows a fully solidified casting (Fig. 4c2), while the solidification rate is the slowest in the case of a constant gas gap width (Fig. 4b2). However, in all three cases, the directional nature of solidification is evident due to the narrow transition zone between the solid and liquid phases. The thermal deformations in the casting for the first simulation scenario are illustrated in Figure 5. A noticeable reduction in the casting's vertical dimension is observed, along with a progressive increase

in the gas gap width. By the end of the solidification process, which occurs at 165 s, the average gap width reaches approximately 0.3 mm, while the vertical dimension of the casting decreases by around 1.6 mm. It is worth noting that the solidification process in the second case was completed after 185 s, while in the third case, it ended after 115 s.

#### 4. Conclusions

The results show the importance of accurately modeling the gas gap to predict heat transfer and solidification dynamics in casting processes. A scenario with near-perfect contact can significantly enhance cooling rates, whereas constant or variable gap widths introduce higher thermal resistance, impacting the rate of solidification. It is possible to achieve a similar solidification time in the case of a constant gap width and a dynamically calculated gap. However, a comparison of the solid phase growth shows significant differences during the earlier stages of the process.

#### References

- [1] Suliga, M., Szota, P., & Mróz, S. (2017). Simulation and measurement of temperature in high speed drawing process of steel wires. *Computer Methods in Materials Science*, 17(1), 69-75. DOI: 10.7494/cmms.2017.1.0577.
- [2] Nishida, Y., Droste, W., & Engler, S. (1986). The air-gap formation process at the casting-mold interface and the heat transfer mechanism through the gap. *Metallurgical Transactions B*, 17, 833-844.
- [3] Florio, B.J., Vynnycky, M., Mitchell, S.L., & O'Brien, S.B.G. (2015). Mould-taper asymptotics and air gap formation in continuous casting. *Applied Mathematics and Computation*, 268, 1122-1139. DOI: 10.1016/j.amc.2015.07.011.
- [4] Mortensen, D., Henriksen, B.R., M'Hamdi, M., & Fjær, H.G. (2016). Coupled modelling of air-gap formation and surface exudation during extrusion ingot DC-casting. in: Grandfield, J.F., Eskin, D.G. (eds). *Essential Readings in Light Metals*. Springer, Cham. DOI: 10.1007/978-3-319-48228-6\_101.
- [5] Zeng, Y.D., Yao, Q.H., & Wang, X. (2017). The effect of air gap between casting and water-cooled mold on interface heat transfer coefficient. *Materials Science Forum*, 893, 174-180, DOI: 10.4028/www.scientific.net/MSF.893.174.
- [6] Ahmadein, M., Pustal, B., Wolff, N., & Bührig-Polaczek, A. (2017). Determination and verification of the gap dependent heat transfer coefficient during permanent mold casting of A356 aluminum alloy. *Material Science & Engineering Technology*, 48(12), 1249-1256, DOI: 10.1002/mawe.201700153.
- [7] Xu, J., Kang, J., Zheng, L., Mao, W., & Wang, J. (2022). Numerical simulation of the directional solidification process with multi-shell mold being gradually immersed in water. *Journal of Materials Research and Technology*, 19, 2705-2716. DOI: 10.1016/j.jmrt.2022.06.037.
- [8] Li, W., Li, L., Geng, Y., Zang, X., Jing, Y., Li, D., & Thomas, B.G. (2021). Air gap measurement during steel-ingot casting and its effect on interfacial heat transfer. *Metallurgical and Materials Transactions B*, 52, 2224-2238. DOI: 10.1007/s11663-021-02152-3.
- [9] Gowsalya, L.A., & Afshan, M.E. (2021). Heat transfer studies on solidification of casting process. in: *Casting Processes and Modelling of Metallic Materials*. DOI: 10.5772/intechopen.95371.

- 
- [10] Węgrzyn-Skrzypczak, E., & Skrzypczak, T. (2024). Numerical modeling of the casting solidification process in a mold taking into account the influence of an air gap with variable width. *Journal of Applied Mathematics and Computational Mechanics*, 23(2), 117-128. DOI: 10.17512/jamcm.2024.2.10.
- [11] Ablaoui, El M., Malendowski, M., Szymkuc, W., & Pozorski, Z. (2023). Determination of thermal properties of mineral wool required for the safety analysis of sandwich panels subjected to fire loads. *Materials*, 16(17), 5852-1 – 5852-18. DOI: 10.3390/ma16175852.